Journal of Ionic Liquids 2 (2022) 100048

Contents lists available at ScienceDirect

Journal of Ionic Liquids

journal homepage: www.elsevier.com/locate/jil

Experimental and theoretical heat capacity of mono- and dicationic long alkyl chain imidazolium-based ionic liquids

Clarissa P. Frizzo[a,*], Jean C.B. Vieira[a], Dineli T.S. Ranathunga[b], Steven O. Nielsen[b], Marcos A. Villetti[c]

[a] Department of Chemistry, Federal University of Santa Maria (UFSM), CEP 97105-900, Santa Maria, RS, Brazil
[b] Department of Chemistry and Biochemistry, University of Texas at Dallas, 800 West Campbell Road, Richardson, TX 75080, United States
[c] Lepol, Department of Physics, Federal University of Santa Maria (Universidade Federal de Santa Maria — UFSM), Santa Maria, Brazil

ARTICLE INFO

Keywords:
Ionic liquid
Imidazolium
Heat capacity
DSC
Molecular modeling

ABSTRACT

Here we present the heat capacity (C_p) of a series of ten imidazolium based ionic liquids (ILs), mono- and dicationic, with chemical formula C_nMIMBr (n = 2, 4, 6, 8, 10, 12, 14, and 16) and $C_n(MIM)_2Br_2$, (n = 4 and 8), respectively. The heat capacity values of eight ILs were determined using modulated differential scanning calorimetry (MDSC) in the temperature range of (358.15 to 378.15) K and compared with the results obtained from theoretical models found in the literature and molecular modeling calculations. For this set of ILs the C_p values were found to be in the range of (189.3 to 985.7) J mol^{-1} K^{-1}. A linear increase in heat capacity with temperature was observed for all ILs. The C_p predicted by theoretical models and molecular modeling calculations showed reasonable agreement with the experimental C_p values for the majority of the studied ILs. The heat capacity increased with the addition of methylene groups in the side and spacer chains for both mono- and dicationic ILs. Consistent with the literature, it is observed that the additional methylene groups have a larger effect on the heat capacity at higher temperature.

1. Introduction

Ionic liquids (ILs) have drawn the attention of chemists due to their unique properties, such as low vapor pressure, high chemical stability and high polarity (Welton, 1999; Wasserscheid and Welton, 2002; Aparicio et al., 2010; Zeng et al., 2017). The main applications of these compounds are in chemical synthesis, catalysis, electrochemistry, separations, and the synthesis of new materials (Welton, 1999; Martins et al., 2014; Hapiot and Lagrost, 2008; MacFarlane et al., 2007; Han and Armstrong, 2007; Zhou and Antonietti, 2003). Some of these applications require information on the thermal properties of these compounds, such as freezing, melting, cold crystallization and glass transition temperatures and their heat capacities. Knowledge about heat capacity (C_p) is vital in the design of physicochemical processes and therefore it is extremely important to obtain C_p values over a wide range of temperatures (Calvar et al., 2013).

There are many experimental techniques available to measure heat capacity (Paulechka, 2010), among which Modulated Differential Scanning Calorimetry (MDSC) is one of the most used due to the possibility of measuring C_p with only one experiment (Diedrichs and Gmehling, 2006). Several works report the heat capacity of ILs as demonstrated by Paulechka in his critical review on the subject (Paulechka, 2010). The majority of these studies comprise monocationic imidazolium-based ILs with anions such as [NTf_2^-], [BF_4^-], [PF_6^-], [OTf^-], and [Br^-]. Data on the heat capacity of long alkyl chain ILs, however, are less common in the literature. These ILs are known for their similarity to surfactants, being able to self-assemble in aqueous solutions forming structures like micelles (Tan et al., 2016). Even scarcer is the data on the heat capacity of dicationic ILs with only a few studies reported in the literature (Kuhn et al., 2020; Zhang, Li and Yang, 2018, 2018; 2019). This emerging class of ILs is known for their higher thermal stability (Anderson et al., 2005; Shirota et al., 2011) and lower toxicity (Steudte, 2014; Moosavi, 2017) than their monocationic analogs.

The heat capacity of some ILs have either not been measured, or are available at just a few temperatures. Besides, due to the tunable properties of ILs, numerous potential ILs can be obtained *via* different cation/anion combinations. Thus, direct experimental determination of the heat capacity of this incredibly high number of ILs over a wide range of operating conditions is unrealistic and unworkable. Therefore, it is essential to explore ways and means of acquiring IL heat capacities in a fast and reliable manner. Molecular modeling is a promising tool for predicting the thermophysical properties of ILs such as heat capacity. As observed in the literature and in the current study, the heat capacity of

* Corresponding author.
E-mail address: clarissa.frizzo@ufsm.br (C.P. Frizzo).

https://doi.org/10.1016/j.jil.2022.100048
Received 8 March 2022; Received in revised form 8 September 2022; Accepted 17 October 2022

ILs can be accurately estimated from the heat capacity of individual ions (Paulechka, 2008). Hence, a wide range of IL combinations with different cations/anion pairs can be tested easily with the molecular modeling protocol used in the current study, for example by varying the anions for the same set of cations. However, at least some experimental data is required to validate and tune the molecular modeling results. Therefore, by combining experiments with computer modeling, researchers can efficiently validate the properties of less studied ILs.

In this work, the heat capacity of a series of ten imidazolium-based ILs, with chemical formula C_nMIMBr (n = 2, 4, 6, 8, 10, 12, 14, and 16) and $C_n(MIM)_2Br_2$ (n = 4 and 8), was determined in the temperature range of (358.15 to 378.15) K. As we are interested in observing the influence of the ILs' alkyl chain length on heat capacity, we chose the anion [$^-$Br] because these ILs can be obtained through simple SN_2 reactions, avoiding anion exchange and purifications. The C_p values measured experimentally were compared with experimental values reported in the literature, with proposed models that predict the heat capacity, and with molecular modeling using classical molecular dynamics simulations for the intermolecular interactions combined with *ab-initio* frequency calculations.

2. Experimental

2.1. Materials and methods

2.1.1. Ionic liquids

The ILs were synthesized by our research group in accordance with procedures that have already been described in the literature (Shirota et al., 2011; Frizzo et al., 2015a). All of the ILs were analyzed by ^{1}H NMR and ^{13}C NMR. Spectral data are presented in the SI and are in accordance with the expected structure. The studied ILs are obtained in an approximately 100 % atom economy synthesis with no impurities in NMR spectra (see spectra in the SI). The amount of water in the IL samples was determined using Karl Fischer titration (detailed information available in the SI).

2.1.2. Equipment

The measurements of heat capacity were performed using an MDSC Q2000 (T-zero^{TM} DSC technology, TA Instruments Inc., New Castle, DE, USA). The cell constant and the temperature calibration were performed by the measurement of the melting point and heat of fusion of an indium sample and less than 1 % deviation from the standard values were observed. Dry high purity (99.999 %) nitrogen gas was used as the purge gas (50 mL min^{-1}). The temperature accuracy is ± 0.1 K, with temperature precision ± 0.01 K, enthalpy precision ± 0.1 %, baseline repeatability ± 10 μW.

2.1.3. Measurement of heat capacities

For the determination of heat capacities (C_p), the samples were crimped in hermetic aluminum pans (100 μL) with lids and a pinhole at the top. The sample mass was that which filled the pan to its maximum capacity, falling in the range of (9 to 20) mg. This sample loading is necessary because the sample size is proportional to the signal. The sample masses were weighed on a Sartorius M 500 P balance to an accuracy of ± 0.001 mg. In this work, the heat capacities of the compounds were determined using modulated DSC. The calibration was performed using the extrapolated onset temperatures and heat of fusion of melting indium, at a heating rate of 10 K min^{-1}. The heating rate used for the samples was 5 K min^{-1}. The samples were subjected to heating in the temperature range (343.15 to 393.15) K. Since at the limits of the temperature range the samples are not fully thermally conditioned, only heat capacities from (358.15 to 378.15) K are presented. Three replicates were carried out for each sample. The DSC curves are shown in the Supporting Information (SI). The accuracy of the DSC equipment in measuring heat capacity was confirmed by determining the C_p of pure water. The values obtained were compared with those from Osborne et al. (1934).

Table 1
Heat capacities of liquid water.

Temperature (K)	Water	
	C_p (J g^{-1} K^{-1})	
	Lit[a]	Exp
303	4.1785	4.52
308	4.1782	4.52
313	4.1786	4.52
323	4.1807	4.53
328	4.1824	4.53
333	4.1844	4.53
AAD%		8.2

[a] Ref [Osborne et al., 1934].

The average absolute percentage deviation (AAD%), defined by Yu and co-workers Yu et al. (2009), was calculated according to Eq. (1), where $C_{p,\mathrm{lit}}$ is the literature value, $C_{p,\mathrm{exp}}$ the experimental value, and n is the number of data points.

$$AAD\% = \frac{1}{n}\sum_{i}^{n}\frac{\left|\left(C_{p,lit} - C_{p,exp}\right)\right|_i}{C_{p,lit}} \times 100 \quad (1)$$

The values of AAD% as well as C_p values for water for a set of temperatures are shown in Table 1. The AAD% value calculated was 8.2 %. Considering that the values used as reference (Osborne et al., 1934) were determined using adiabatic calorimetry, which has a much lower uncertainty than DSC (Paulechka, 2010), the AAD% value was considered acceptable.

2.1.4. Computational details

For the molecular modeling study the isobaric heat capacity (C_p) is obtained directly from its definition (Eq. 2) because the heat capacity estimated using the statistical mechanics fluctuation formula is reported to cause large deviations (Cadena et al., 2006),

$$C_p(T,P) = \left(\frac{\partial\langle H\rangle}{\partial T}\right)_p \quad (2)$$

Namely, C_p is determined from the slope of the enthalpy versus temperature graph. As described in Cadena et al. (2006) and shown in several other studies (Kuhn et al., 2020; Liu et al., 2012; Sprenger et al., 2015) to obtain accurate values, C_p is divided into two parts, namely the residual portion and the ideal gas portion (Eq. (3)). The residual portion of the heat capacity considers all the intermolecular interactions while the ideal gas portion takes into account the intramolecular interactions (Cadena et al. 2006).

$$C_p(T,P) = C_p^{RES} + C_p^{IG} = \left(\frac{\partial\langle H_{RES}\rangle}{\partial T}\right)_p + \left(\frac{\partial\langle H_{IG}\rangle}{\partial T}\right)_p \quad (3)$$

Where $H_{RES} = \Phi^{NB} + PV - Nk_BT$ (where Φ^{NB} is the non-bonded energy, P is the pressure, V is the volume, N is the number of molecules, k_B is the Boltzmann constant and T is the temperature) and $H_{IG} = \Phi^{INT} + KE + Nk_BT$ (where Φ^{INT} is the bonded energy and KE is the kinetic energy) (Cadena et al., 2006).

In theory, classical molecular dynamics (MD) simulations at finite temperatures can be used to obtain both of these contributions, and are known to handle very large molecules with considerable accuracy (Theodorakis et al., 2011; Frenkel and Smith, 1996). However, for the size of molecules considered here, it is reported that classical MD simulation does not take into account the intramolecular interactions correctly (Fakhraee et al., 2014; Fakhraee and Gholami, 2015; Doherty et al., 2017). Therefore, only the residual contribution of the heat capacity (Cp^{RES}) is determined using classical MD simulations. As suggested in the literature, the ideal gas contribution (Cp^{IG}) is calculated from ab initio frequency analysis with appropriate vibrational scaling.Liu et al. (2012), Sprenger et al. (2015), Kuhn et al. (2020) In the current study, Cp^{RES} is calculated from the slope of the residual

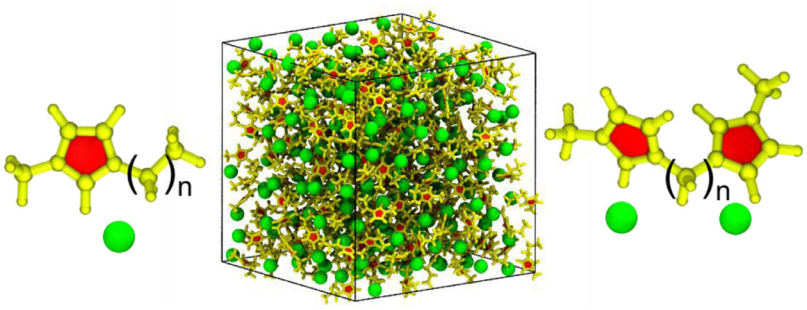

Fig. 1. Imidazolium-based mono- and dicationic ionic liquids with bromide anions (green) investigated in this study. For monocationic ILs n = 1, 3, 5, 7, 9, 11, 13, 15 and for dicationic ILs n = 4, 8 were studied.

enthalpy versus temperature graphs obtained from classical MD simulations and Cp^{IG} is obtained from ab initio thermochemistry calculations following the above equations. The all atom MD computer simulations were performed using the NAMD software package (v.2.13) (Phillips et al., 2005). All the trajectories were visualized using the VMD software package (Humphrey et al., 1996). The cation parameters were obtained from Gross et al. (2011) and the anion parameters were taken from other published works (Doherty et al., 2017; Lopes and Pádua, 2006; Kohagen et al., 2011; Kam et al., 2019). We also calculated the heat capacity of pure water using the TIP3P water model (Kuhn et al., 2020; Vega and Abascal, 2011; Neverov and Komolkin, 2010; Johnson III, 2020). Although the non-polarizable models have provided important insights into molecular-level structure and correlations in ionic systems, they are also known to have some limitations showing much slower dynamics and some disagreement with experiments at higher salt concentrations (Bedrov et al. 2019; Ishii et al., 2022, 2020; Hernández-Ríos et al., 2017). The use of polarizable force fields in simulations generally shows better agreement with experiments. However, considering the high computational cost of using polarizable force fields in ionic liquid systems (Yan et al., 2004) and their unavailability for some of the ions considered in the current study, non-polarizable force fields were used with scaled atomic charges. The atomic charge scaling method with non-polarizable force fields is a well-known method in MD simulations to account for charge transfer and polarization effects, with the goal of reducing computational cost and guaranteeing the stability of numerical integration (Yan et al., 2004; Nasrabadi and Gelb, 2017; Dommert et al. 2012). Furthermore, this rescaling of ionic charge in non-polarizable classical MD simulations has been shown to improve the prediction of heat capacity and provide a satisfactory molecular description (Chaban et al., 2011; Sprenger et al., 2015; Bedrov et al. 2019; Ren et al. 2004; Dommert et al. 2012). A charge scaling factor of 0.8 is used to scale the atomic partial charges, which was reported in several previous MD studies to accurately predict the known experimental heat capacity of imidazolium-based ionic liquids (Yan et al., 2004; Nasrabadi and Gelb, 2017; Zhong et al., 2011; Mondal and Balasubramanian, 2014; Chaban et al., 2011; Youngs and Hardacre, 2008). To prepare the initial configurations a (50 × 50 × 50) $\forall^3$ unit cell (Fig. 1) with 250 randomly placed ion pairs was generated using Packmol (Martínez et al., 2009) for each system and periodic boundary conditions were applied in all three directions. For the dicationic systems (Di-C_nMIMBr_2) 250 cations and 500 anions were used. These systems were relaxed by conjugate gradient energy minimization followed by a canonical (NVT) simulation for 10 ns at 300 K. To equilibrate the system density and overcome energy traps due to the slow dynamics of ionic liquids, annealing simulations were carried out by heating the system up to 700 K (Kuhn et al., 2020; Nasrabadi and Gelb, 2017; Zhong et al., 2011; Mondal and Balasubramanian, 2014; Chaban et al., 2011; Youngs and Hardacre, 2008; Tenney et al., 2014) and cooling step by step in 2 K decrements to the target temperature over 10 ns under isobaric–isothermal conditions (NPT) at a pressure of 1 atm. After this procedure twelve independent NPT simulations were performed each for 50 ns at different target temperatures for each system. The ionic liquid systems were simulated at temperatures ranging from (358 to 380) K, and the water simulations were carried out at temperatures ranging from (302 to 344) K, by considering the temperatures used in the experiments. A 12 Å cutoff was used for the van der Waals and short-ranged electrostatics interactions, while the long-range electrostatics were treated with the Particle Mesh Ewald technique. The last 30 ns of the trajectory is used to calculate the average enthalpy for each system. A graph of the residual enthalpy ($H_{RES} = \Phi^{NB} + PV - Nk_BT$) versus temperature is plotted (Figs. S33 and S34), and the residual portion of the heat capacity was obtained from its slope. Following Liu et al. (2012), it is assumed that the residual contribution to the heat capacity is constant within the selected temperature range. To obtain the ideal gas contribution to the heat capacity, ab initio thermochemistry calculations were performed using the Gaussian 16 package (Frisch et al., 2016). Since the CPU time increases rapidly with the increase in the size of molecule, for larger molecules a suitable algorithm that gives a balance between the computational time and accuracy is needed. Following Hennemann et al. (2018) and Vieira et al. (2020) we studied several ab initio methods for the considered set of molecules and found the closest agreement between theory and experiment for B3LYP/aug-cc-pVDZ with suitable scaling factors. Paulechka et al. (2008), Hennemann et al. (2018), Vieira et al. (2020), Curtiss et al. (1998) Therefore, considering the computational cost, time and accuracy we decided to use the B3LYP/aug-cc-pVDZ (Paulechka et al., 2008; Hennemann et al., 2018; Vieira et al., 2020) level of theory for both ion pairs (Paulechka et al., 2008; McDaniel et al., 2016) and for isolated ions ($C_p = C_{p,\text{cation}} + C_{p,\text{anion}}$) (Paulechka et al., 2008) to perform geometry optimization followed by frequency analysis. To start these calculations, we placed the bromide ion(s) above the plane of the imidazolium ring(s) following the most stable configurations reported in Turner et al. (2003). Optimized structures are shown in Fig. S35. The ideal gas heat capacities at different temperatures were analyzed from the thermochemistry output using a perl script (Hernández-Ríos et al., 2017; Irikura, 2002) (for ideal gases, $C_p = C_v + R$). Typically, ab-initio vibrational frequencies show some disagreement with experimental data due to anharmonicity, basis set truncation, and incomplete incorporation of electron correlation. Frequency scaling is one of the often-applied methods in the literature to compensate for the deviation between the calculated and the experimental observed results (Červinka and Beran, 2017; Paulechka et al., 2007; Crosthwaite et al., 2005). Small molecules with a number of atoms <40 show good agreement to experiments with no requirement for frequency scaling. However, for large molecules with a number of atoms > 40, we identify the optimal scaling value for each system to align the calculated heat capacity with the linear trend observed for the ILs with <40 atoms (n≤8) in Fig. 4b over the considered temperature range (see Fig. S36). (Červinka and Beran, 2017). All the scaling factors used and the ideal gas and residual heat capacities obtained are given in Tables S3 and S4.

3. Results and discussion

3.1. Experimental heat capacity

Heat capacities of eight imidazolium-based ILs were measured from (343.15 to 393.15) K. However, only data from (358.15 to 378.15) K are

Table 2
Molar heat capacities ($C_{p,m}$) of the studied ionic liquids from (358.15 to 378.15) K.

T (K)	$C_{p,m}$ for ILs CnMIMBr and Di-CnMIMBr$_2$ (J mol^{-1} K^{-1})							
	n = 2	n = 4	n = 6	n = 8	n = 12	n = 16	Di n = 4	Di n = 8
358.15	189.3 ± 2.9[a]	294.1 ± 29	400.5 ± 1.4	540.2 ± 8.5	706.8 ± 0.9	924.4 ± 16	645.9 ± 0.6	773.5 ± 6.2
359.15	189.5 ± 2.2	295.0 ± 30	401.3 ± 1.3	541.8 ± 8.3	707.6 ± 0.3	929.1 ± 17	647.5 ± 0.8	775.6 ± 6.3
360.15	189.7 ± 2.0	295.5 ± 31	402.1 ± 1.6	543.2 ± 8.2	710.1 ± 1.8	932.1 ± 17	649.6 ± 1.2	777.8 ± 6.2
361.15	189.8 ± 1.5	296.4 ± 32	402.7 ± 1.3	544.1 ± 8.1	711.7 ± 0.6	935.1 ± 16	651.3 ± 0.7	779.2 ± 6.3
362.15	190.1 ± 1.1	297.1 ± 33	403.5 ± 1.6	545.2 ± 8.4	712.8 ± 0.6	938.5 ± 17	653.0 ± 0.6	780.8 ± 6.6
363.15	190.1 ± 1.1	297.7 ± 34	404.2 ± 1.7	546.9 ± 8.1	714.6 ± 0.9	941.2 ± 17	654.5 ± 0.8	782.6 ± 6.6
364.15	190.3 ± 0.9	298.5 ± 35	404.5 ± 1.7	547.9 ± 8.3	715.6 ± 0.5	944.4 ± 18	655.8 ± 0.8	784.3 ± 6.7
365.15	190.5 ± 0.8	299.1 ± 36	405.2 ± 1.8	549.7 ± 8.1	716.8 ± 0.8	946.6 ± 17	657.3 ± 0.6	785.6 ± 6.4
366.15	190.5 ± 0.4	299.8 ± 38	405.8 ± 1.7	550.8 ± 8.3	718.1 ± 0.6	949.6 ± 18	658.6 ± 1.0	787.3 ± 6.5
367.15	190.7 ± 0.5	300.7 ± 39	406.2 ± 1.6	551.4 ± 8.1	719.5 ± 0.7	952.7 ± 18	659.8 ± 0.9	788.5 ± 6.5
368.15	190.7 ± 0.5	301.4 ± 41	406.6 ± 1.8	553.4 ± 8.0	721.4 ± 0.5	955.1 ± 18	661.1 ± 0.8	790.4 ± 6.2
369.15	190.8 ± 0.4	302.1 ± 42	407.4 ± 2.0	554.4 ± 7.8	722.5 ± 0.7	958.6 ± 19	662.1 ± 0.8	791.7 ± 6.6
370.15	191.0 ± 0.5	302.8 ± 44	407.6 ± 1.6	556.0 ± 8.2	724.1 ± 0.5	961.7 ± 19	663.9 ± 0.8	793.3 ± 6.2
371.15	191.0 ± 0.7	303.8 ± 45	407.8 ± 2.1	557.7 ± 7.8	725.0 ± 0.4	964.6 ± 19	665.1 ± 0.9	795.4 ± 6.0
372.15	191.2 ± 0.6	304.6 ± 47	408.4 ± 1.6	559.0 ± 7.9	726.5 ± 0.5	967.3 ± 19	666.3 ± 0.9	797.0 ± 6.5
373.15	191.3 ± 0.6	305.7 ± 49	408.7 ± 2.1	560.3 ± 8.0	728.0 ± 0.5	970.6 ± 19	667.5 ± 1.0	798.3 ± 5.5
374.15	191.5 ± 0.7	306.6 ± 50	409.3 ± 2.2	562.0 ± 8.4	729.3 ± 0.3	973.2 ± 19	669.1 ± 0.9	800.7 ± 5.7
375.15	191.4 ± 0.8	307.8 ± 52	409.6 ± 2.5	564.2 ± 8.1	730.9 ± 0.6	976.5 ± 19	670.4 ± 1.2	802.4 ± 5.4
376.15	191.5 ± 0.7	309.1 ± 54	409.9 ± 2.2	565.3 ± 7.8	732.2 ± 0.3	979.8 ± 20	671.2 ± 1.3	804.1 ± 5.6
377.15	191.8 ± 0.9	310.5 ± 56	410.5 ± 2.1	567.5 ± 8.2	733.4 ± 0.4	982.9 ± 20	672.8 ± 1.1	806.3 ± 5.9
378.15	191.6 ± 1.0	311.9 ± 58	410.7 ± 2.2	569.0 ± 8.0	734.8 ± 0.3	985.7 ± 20	674.1 ± 1.2	808.7 ± 5.5

[a] Uncertainty expressed as standard uncertainty of the mean in J mol^{-1} K^{-1}.

presented since at the outer limits of the temperature range the samples are not fully thermally conditioned. To measure the heat capacities of the ILs, it is important to ensure that these compounds do not show first order phase transitions in the temperature range of the reported C_p data, since the C_p at first order phase transitions goes to infinity. None of the studied ILs exhibit first order phase transitions from (358.15 to 378.15) K. The ILs C_2MIMBr and C_4MIMBr have melting points at 350 K and 351 K, respectively (Paulechka et al., 2007), so these ILs are in the liquid state at the reported temperature range. The ILs C_6MIMBr and C_8MIMBr do not show phase transitions except for a glass transition at very low temperature (Crosthwaite et al., 2005; Bender, 2014). The IL C_{12}MIMBr has a well-studied thermal behavior and does not show phase transitions from (358.15 to 378.15) K (Bender et al., 2019; Inoue et al., 2007). The IL C_{16}MIMBr also does not show phase transitions in this temperature range (Zhu et al., 2009). The dicationic IL Di-C_4MIMBr$_2$ has a melting point at 388.15 K (Zhang, Li and Yang, 2018), being solid in the temperature range used in this study. Finally, the dicationic IL Di-C_8MIMBr$_2$ has a melting point at 343.15 K (Gindri et al., 2014; Frizzo et al., 2015b). The influence of the physical state of the IL samples in C_p is that liquids tend to have much higher C_p than solids, that is because liquids have more freedom of movement and, consequently, more energy is necessary to raise the temperature of a liquid sample compare to a solid one (Bendová et al., 2020). Regarding the ILs C_{10}MIMBr and C_{14}MIMBr, we could not obtain reproducible MDSC measurements for the determination of C_p in the temperature interval (343.15 to 393.15) K. The results of the C_p measurements are summarized in Table 2 in terms of the molar heat capacity, $C_{p,m}$.

An important aspect of heat capacity measurements is the presence of impurities in the sample, which can affect the measured values. The most prominent impurity that can shift the C_p values is water (Paulechka, 2010; Paulechka et al., 2010). In the present study, the temperature range of the reported C_p includes a water phase transition temperature (373.15 K) yet no anomalous behavior is observed close to this temperature. Thus, it is reasonable to assume that the IL samples do not present an amount of bulk water detectable by DSC analysis, which does not mean that the samples are completely free of water. In fact, the amount of water detected by Karl Fischer titration was, in the range of 1.4 ± 0.3 - 6.32 ± 0.01% (see Table S6 for the values for each IL). The amounts of water detected were considered to be acceptable for practical uses of these ILs, since the absorption of water is inevitable and drying the materials consumes a lot of time and resources. The value found here is close to the 4.5 % of water content for the IL [C_{16}MIM][Cl] used in C_p measurements by Bendová et al. (2020).

There are a few reports of $C_{p,m}$ of ILs at high temperatures such as above 350 K. Paulechka et al., 2007 reported the $C_{p,m}$ of the ILs C_2MIMBr and C_4MIMBr at 360 K as equal to 269 J mol^{-1} K^{-1} and 336 J mol^{-1} K^{-1}, respectively. These values are 42 % and 14 % higher than the values reported here, however, different techniques were used to measure the $C_{p,m}$, which could explain this considerable difference. Besides, we have obtained a considerable uncertainty in the results for C_4MIMBr, so differences between this work and literature may be expected. The same difference in $C_{p,m}$ for C_4MIMBr (14 %) was observed comparing with the work of Hu et al. (2011). These differences in $C_{p.m}$ may also arise from the different amounts of water in the samples, which are higher in the present work. The presence of water is known to elevate the measured values of $C_{p.m}$ (Paulechka et al., 2007), however, it can be seen that the values obtained here are lower than those reported with lower amounts of water, which indicates that this is not the major factor influencing the differences. Considering the IL C_{16}MIMBr, the $C_{p,m}$ values at 358 K were reported by Zhu et al. (2009) and deviate from the values reported here by only 2.5 %, despite the IL C_{16}MIMBr used in the present work presenting an amount of water of 4.6 % in comparison with less than 0.05 % in the cited reference. The heat capacity of the dicationic IL Di-C_4MIMBr$_2$ has been reported in the literature (Zhang et al., 2019), but the authors did not specified the temperature corresponding to the published value, making it hard to compare with the present work.

Generally speaking, the heat capacity of ILs is related to their molecular mass where the larger the mass, the greater the heat capacity. Typically, the increase of heat capacity with increasing temperature is fit to a polynomial function. However, in this work, a linear relation between molar heat capacity and temperature ($C_{p,m}$ = aT + b) was used because the values of the correlation coefficient (r) are all higher than 0.99. A plot of $C_{p,m}$ versus temperature is shown in Fig. 2. The fitting parameters can be seen in Table 3 along with the predicted values of $C_{p,m}$ at 298.15 K extrapolated from the linear fit.

The $C_{p,m}$ at 298.15 K predicted using the linear equation from Table 3 can be compared to the $C_{p,m}$ literature values reported at 298.15 K (Crosthwaite et al., 2005) for the ILs C_6MIMBr and C_8MIMBr. Our results of 372 J mol^{-1} K^{-1} and 455 J mol^{-1} K^{-1} for the ILs C_6MIMBr and C_8MIMBr, respectively, are 7.8 % higher than the literature for the IL C_6MIMBr and 16 % higher for the IL C_8MIMBr. Considering the IL C_4MIMBr, the calculated $C_{p,m}$ of 243 J mol^{-1} K^{-1} at 298.15 K was found

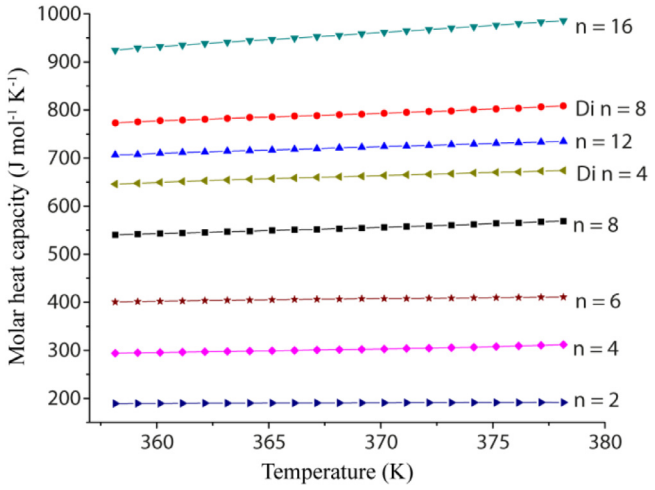

Fig. 2. Experimental molar heat capacities (J mol^{-1} K^{-1}) as a function of temperature (K) for the studied ionic liquids C_nMIMBr and Di-C_nMIMBr$_2$.

Table 3
Fitting parameters for the linear fit of the $C_{p,m}$ dependence on temperature, correlation coefficients (r), and the extrapolated $C_{p,m}$ value at 298.15 K.

IL	$C_{p,m}$ = aT + b		$C_{p,m}$ at 298.15 K	
	a	b	r	(J mol^{-1} K^{-1})
C_2MIMBr	0.118	147.07	0.990	182
C_4MIMBr	0.844	-8.6123	0.993	243
C_6MIMBr	0.493	224.71	0.992	372
C_8MIMBr	1.412	34.119	0.998	455
C_{12}MIMBr	1.394	207.75	0.999	623
C_{16}MIMBr	2.986	-143.65	0.999	747
Di-C_4MIMBr$_2$	1.373	155.32	0.998	565
Di-C_8MIMBr$_2$	1.683	171.16	0.999	673

to be very similar to the 241.8 J mol^{-1} K^{-1} reported in the work of Paulechka et al., 2007 at the same temperature. However, the calculated value was 23 % lower than reported by Kim et al., 2004a, 2004b) and 30 % lower than $C_{p,m}$ reported by Fredlake et al. (2004). These differences in $C_{p,m}$ may be caused by the greater amount of water in the samples studied here, although the $C_{p,m}$ at 298.15 K for C_4MIMBr is very close to the reported in the literature (Paulechka et al., 2007) despite the later having a much lower water content (0.14 %).

3.2. Predictive models of heat capacity

The heat capacities of the IL studied here have been predicted using the models available in the literature. There are various proposed models to predict heat capacities, such as the recent hybrid group method of data handling developed by Rostami *et al.* (Rostami et al., 2019), however, this method requires a great number of calculations and, therefore, a considerable amount of computational time. Other methods, although older, are simpler and give fairly good results. One of these methods was developed by Gardas and Coutinho (2008). This method consists in a second order group additivity technique applied to 19 ILs composed of several cations and anions, including imidazolium and bromide, with a total of 2400 data points. Another method was developed by Farahani et al. (2013), consisting of a 5-term temperature dependent correlation utilizing molecular parameters for a total of 56 ILs and 2490 data points. The method developed by Ahmadi et al. (2015) is based on a dataset of 128 ILs, consisting of 4822 data points, and utilizes as input temperature, molecular mass and the number of atoms in the IL. These models are developed and validated considering a great number of experimental values, thus the results are considered to be in fairly good agreement with reality. Considering the viability of the last three methods, the heat capacities of the C_nMIMBr and Di-C_nMIMBr$_2$ were predicted using these models and compared with heat capacity values measured in this work. Percentage deviations of the experimental values from the predictions for monocationic ILs are given in Table 4. Considering the three methods, the deviation observed in the experimental value was negative for the ILs with shorter side chains, i.e., the predicted value is higher than the experimental value. The experimental heat capacities of C_6MIMBr, at different temperatures, have a small deviation from that predicted by the Gardas and Coutinho, and Farahani, methods. The values of the heat capacity obtained for C_8MIMBr from the Ahmadi method agreed well with the experimental values. On the other hand, for ILs with larger side alkyl chains, the deviation observed was positive, i.e., the experimental value is higher than the predicted value. For the dicationic ILs, a good fit between the experimental and predicted values for the Gardas and Coutinho, and Ahmadi, methods was observed, as shown in Table 5. The values obtained from Faharani's method, however, deviate considerably from the experimental ones. Although there are some considerable deviations between predicted and experimental

Table 4
Deviation of the experimental values from the prediction for the monocationic ILs C_nMIMBr.

n	Deviation (%)				
	358.15 K	363.15 K	368.15 K	373.15 K	378.15 K
	Gardas and Coutinho				
2	-29.5	-29.8	-30.2	-30.6	-31.1
4	-13.4	-13.1	-12.7	-12.2	-11.2
6	-2.6	-2.5	-2.7	-2.9	-3.3
8	+11.9	+12.5	+12.9	+13.5	+14.3
12	+13.0	+13.4	+13.6	+13.9	+14.1
16	+20.3	+21.6	+22.5	+23.6	+24.7
	Farahani				
2	-23.7	-24.1	-24.6	-25.0	-25.5
4	-9.6	-9.1	-8.6	-8.0	-6.7
6	-0.4	-0.1	-0.1	-0.1	-0.2
8	+12.7	+13.6	+14.4	+15.3	+16.5
12	+11.6	+12.4	+13.1	+13.7	+14.4
16	+30.1	+32.1	+33.6	+35.3	+37.0
	Ahmadi				
2	-42.4	-42.6	-42.8	-43.0	-43.3
4	-24.9	-24.4	-23.9	-23.2	-22.1
6	-11.9	-11.5	-11.4	-11.4	-11.4
8	+3.7	+4.5	+5.3	+6.1	+7.3
12	+9.6	+10.4	+11.1	+11.7	+12.3
16	+19.6	+21.4	+22.8	+24.4	+26.0

Table 5
Deviation of the experimental values from the prediction for the dicationic ILs Di-C_nMIMBr$_2$.

n	Deviation (%)				
	358.15 K	363.15 K	368.15 K	373.15 K	378.15 K
	Gardas and Coutinho				
4	+6.2	+6.7	+6.9	+7.0	+7.1
8	+3.0	+3.4	+3.6	+3.8	+4.2
	Farahani				
4	+23.4	+24.5	+25.2	+25.9	+26.6
8	+14.2	+15.1	+15.9	+16.7	+17.8
	Ahmadi				
4	+3.2	+4.2	+4.9	+5.5	+6.2
8	+2.5	+3.4	+4.1	+4.8	+5.9

Table 6
Simulated molar heat capacities of the ionic liquids.

	Simulated $C_{p,m}$ for ILs C_nMIMBr and Di-C_nMIMBr$_2$ (J mol^{-1} K^{-1})									
T (K)	n = 2	n = 4	n = 6	n = 8	n = 10	n = 12	n = 14	n = 16	Di n = 4	Di n = 8
358	213.84	308.12	400.53	503.82	604.43	709.07	814.54	931.72	634.34	779.56
360	214.71	309.23	402.03	505.63	606.77	711.82	817.60	935.12	636.25	782.12
362	215.58	310.34	403.53	507.43	609.09	714.56	820.65	938.50	638.15	784.67
364	216.45	311.46	405.02	509.23	611.41	717.28	823.68	941.86	640.05	787.20
366	217.33	312.57	406.52	511.03	613.72	720.00	826.70	945.21	641.93	789.73
368	218.20	313.68	408.01	512.83	616.02	722.70	829.70	948.54	643.81	792.24
370	219.08	314.80	409.50	514.62	618.32	725.38	832.69	951.86	645.67	794.73
372	219.95	315.91	410.99	516.42	620.60	728.06	835.66	955.16	647.53	797.22
374	220.82	317.02	412.48	518.21	622.88	730.72	838.62	958.44	649.37	799.69
376	221.70	318.14	413.96	520.00	625.14	733.37	841.57	961.71	651.21	802.15
378	222.57	319.25	415.45	521.78	627.40	736.00	844.50	964.96	653.03	804.59
380	223.45	320.37	416.93	523.57	629.65	738.63	847.41	968.20	654.85	807.03

C_p, the coefficient of determination (R^2) of the curves of predicted value as a function of the experimental one (not shown), at the temperatures shown in Tables 4 and 5, are all ≥ 0.975 (see Table S5), showing that there is a good linear correlation between predicted and experimental values as temperature increases.

3.3. Molecular modeling calculation of heat capacity

To further investigate the reliability of the measured heat capacities in this work, a molecular modeling analysis was performed and the computational data was compared with those measured using MDSC. First, to validate the computational method, the C_p of TIP3P water was measured at temperatures ranging from (302.0 to 344.0) K and the results are listed in Table S1. The data shows a good agreement with the literature (Sprenger et al., 2015; Neverov and Komolkin, 2010; Johnson III, 2020); we therefore conclude that the computational methodology yields accurate results. The constant pressure heat capacities of all ionic liquids were calculated following the same procedure at temperatures ranging from (358.0 to 380.0) K.

It is known that ab-initio vibrational frequencies typically show some disagreement with experiments. Frequency scaling is one of the methods commonly applied to compensate these deviations (Červinka and Beran, 2017; Sinha et al., 2004; Roy and Gerber, 2013). For the smallest molecule tested (C_2MIMBr), it was observed that the B3LYP/aug-cc-pVDZ method overestimates the $C_{p,m}$, showing a negative deviation from the experiments (Table S4). For large molecules with a number of atoms >40, B3LYP/aug-cc-pVDZ underestimates the $C_{p,m}$ by about 20 % (unscaled data in Table S4), suggesting that the calculated vibrational frequencies are overestimated. The precalculated scale factor of 0.974 (Irikura, 2002) consistent with the B3LYP/aug-cc-pVDZ level of theory was observed to show <15 % deviation from the experiments. Therefore, following Červinka and Beran (2017) linear frequency scaling corrections were applied (Červinka and Beran, 2017; Paulechka et al., 2007; Roy and Gerber, 2013; Scott and Radom, 1996). Fig. S36 shows the sensitivity of the $C_{p,m}$ to the scaling of the vibrational frequencies.

It is expected that the molar heat capacity increases linearly in proportion both to the number of –CH2– functional groups and the molecular mass. This linear correlation between $C_{p,m}$ with chain length and molecular mass was clearly observed when the number of atoms in the cation is ≤40 (Figs. 4b and 5b, results will be discussed in detail in Section 3.4). At the same time, a good agreement was found between the calculated heat capacities of these ILs (with a number of atoms in the cation ≤40) and the experiments. (Table S4) (Roy and Gerber, 2013). Therefore, unscaled (scaling factor 1) vibrational frequencies were used for the C_2MIMBr, C_4MIMBr, C_6MIMBr and C_8MIMBr systems. Although a scaling factor of 0.974 shows the best fit to the experimental anomaly in the $C_{p,m}$ of the C_8MIMBr system (Fig. S36), the unscaled data yields the best linearity between $C_{p,m}$ with chain length and molecular mass. For the IL C_{10}MIMBr (number of atoms in the cation is 46) which lacks experimental data, a best fit to the linear trend was achieved by a scaling of 0.8 (Table S3). To be consistent with the linear trend of $C_{p,m}$ with chain length and molecular weight, appropriate scaling factors (Table S3) were used for ILs with number of atoms >46 (C_{10}MIMBr, C_{12}MIMBr, C_{14}MIMBr, C_{16}MIMBr, Di-C_4MIMBr$_2$ and Di-C_8MIMBr$_2$). A systematic investigation yielded an optimal scaling value of 0.70, resulting in a linear trend of heat capacity, with <3% deviation from the experiment for ILs with number of atoms in the cation >46 over the selected temperature range (Table S4). The final heat capacities calculated through molecular modeling are in Table 6 and show good agreement with the experimental results. Altogether, with appropriate quantum corrections, the experimental heat capacities were well-reproduced (<3.5 % deviation) through molecular modeling (Table S4). Specifically, unscaled vibrational frequencies are used for ILs with a small number of atoms (number of atoms ≤40), while appropriate vibrational frequency scaling factors are used for ILs with a large number of atoms (number of atoms >40). To be clear, the vibrational frequency scaling factors were selected to achieve a linear trend in $C_{p,m}$ with chain length and molecular mass and not to fit the experimental data. This molecular modeling technique can be used to predict the heat capacities of other ILs lacking experimental results (as tested for C_{10}MIMBr, C_{14}MIMBr).

Fig. 3 shows the final calculated heat capacities of all ILs modeled, along with the experimental values. The residual portion of the $C_{p,m}$ obtained from the enthalpy vs temperature graphs (Fig. S33) are reported in Table S2 and the ideal gas $C_{p,m}$ of the ion-pairs and individual ions derived from ab initio calculations are presented in Table S3. Similar to Paulechka et al. (2008) we did not observe a significant change between the ideal gas $C_{p,m}$ values obtained for the ion pairs vs the individual ions (see Fig. 3). The highest percentage deviation observed is 4.4 % for the Di-C_8MIMBr$_2$ system (see Fig. 3). One possible reason for observing the largest deviation in the dicationic system could be that when ion pairs are used, the imidazolium cation could be affected by the asymmetric electric field caused by the neighboring bromide single point charges. The ion pairs predict heat capacities closer to the experiments than the individual ion results (Fig. 3).

When the deviations in Tables 4 and 5 (experimental data vs. predictive models) are compared with the deviations in Table S4 (experimental data vs. computational results) it is clear that the computational procedure is an improvement over the predictive models. In reality the heat capacity comes predominantly from the vibrational modes of the molecules. The vibrational modes span a wide frequency range from fully thermalized (thus contributing R to heat capacity) to unthermalized (contributing nothing), which would be difficult to predict. Since these modes are directly computed with an ab initio method, and moreover the intermolecular contribution to the heat capacity is directly computed from MD simulation, we could improve upon the predictive models albeit at a higher computational cost.

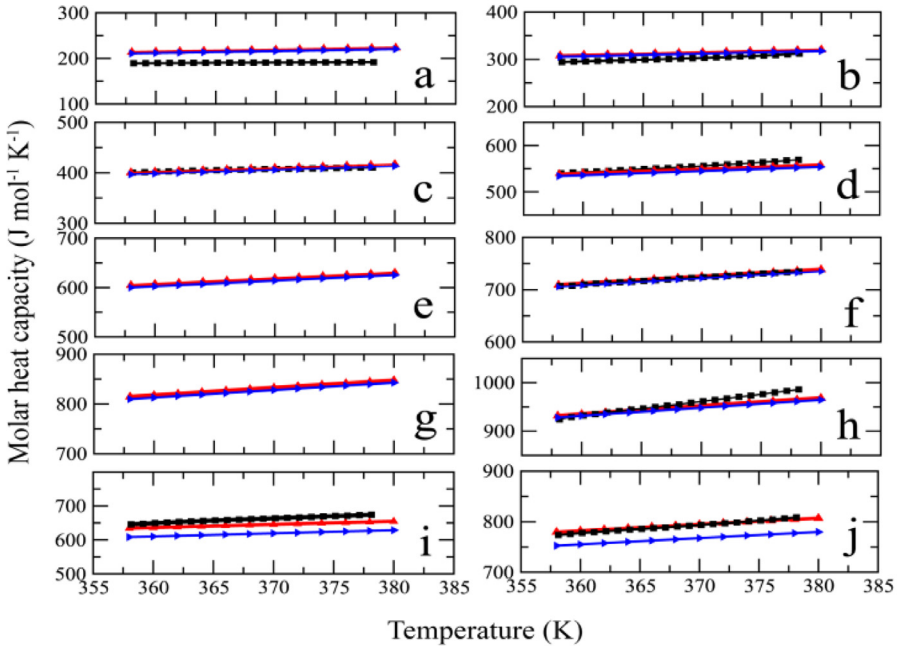

Fig. 3. Comparison of isobaric molar heat capacities (J mol^{-1} K^{-1}) as a function of temperature (K) calculated by computer simulations with experiments for the studied ILs C_2MIMBr (a), C_4MIMBr (b), C_6MIMBr (c), C_8MIMBr (d), C_{10}MIMBr (e), C_{12}MIMBr (f), C_{14}MIMBr (g) C_{16}MIMBr (h), Di-C_4MIMBr$_2$ (i) and Di-C_8MIMBr$_2$ (j). Coloring is as follows: experimental C_p (black, ■), simulated C_p of ion pairs (red, ▲) and simulated C_p of individual ions (blue, ►).

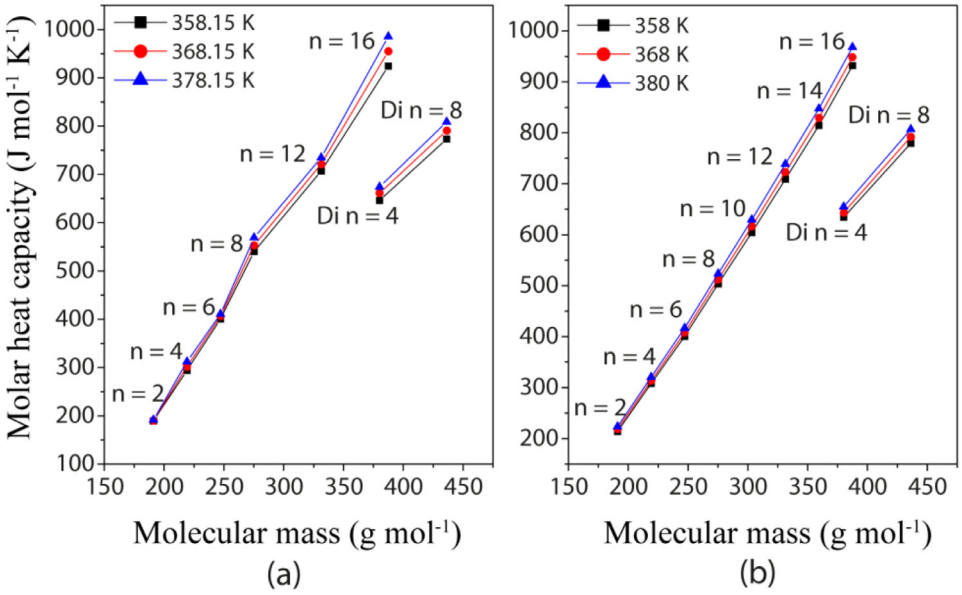

Fig. 4. **(a)** Experimental molar heat capacities (J mol^{-1} K^{-1}) as a function of molecular mass (g mol^{-1}) for the studied ILs C_nMIMBr and Di-C_nMIMBr$_2$ at 358.15 K, 368.15 K and 378.15 K. **(b)** Molecular modeling molar heat capacities (J mol^{-1} K^{-1}) as a function of molar mass (g mol^{-1}) for the studied ILs C_nMIMBr and Di-C_nMIMBr$_2$ at 358 K, 368 K, and 380 K.

3.4. Heat capacity as a function of molecular mass and chain length

To study how the $C_{p,m}$ changes with molecular mass and length of the alkyl chain at different temperatures we construct the graphs of $C_{p,m}$ vs molar mass and $C_{p,m}$ as a function of the number of –CH_2– groups using both experimental and computational results. We observed a good agreement between the experimental and computational results with both following the same trend. Here only the computational heat capacities obtained for ion pairs were plotted to reduce clutter.

When we study the trend of $C_{p,m}$ in relation to molecular mass, we can see that the dicationic IL Di-C_4MIMBr$_2$ has a greater molecular mass and lower $C_{p,m}$ than C_{12}MIMBr. The same is true for the IL Di-C_8MIMBr$_2$ in relation to C_{16}MIMBr (see Fig. 4a,b). Based on this, it would be reasonable to assume that there are other aspects besides molecular mass affecting the heat capacities of the ionic liquids, particularly for dicationic ILs. In the case of the class of ILs studied here, the higher values of $C_{p,m}$ for the dicationic in relation to the corresponding monocationic ILs is a trend already reported in the literature (Zhang et al. (2018, 2019). This results from the fact that the heat capacity depends on the number of vibrational, translational, and rotational modes for energy storage in the molecules (Zhang et al., 2018, 2019). Thus, molecules with more modes should have higher heat capacities, as is the case for dicationic ILs compared to their monocationic counterparts. This trend can be clearly seen in the results of this work comparing the values of $C_{p,m}$ of the dicationic ILs Di-C_4MIMBr$_2$ and Di-C_8MIMBr$_2$ with those of the monocationic ILs C_4MIMBr and C_8MIMBr. This effect also helps to explain the lower $C_{p,m}$ of dicationic ILs in relation to C_{12}MIMBr and C_{16}MIMBr. Since bromide anions only have translational modes, they do not contribute to $C_{p,m}$ as much as the cations. The molecular mass of $C_{12}MIM^+$ and $C_{16}MIM^+$ cations are higher than those of dications Di-C_4MIM^{2+} and Di-C_8MIM^{2+}, so there is a correspondence between the molecular mass of the cation and $C_{p,m}$.

The effect of the addition of –CH_2– groups on the side chain of the ILs was determined by plotting the $C_{p,m}$ values of ILs with $n = 2$ to $n = 16$ as a function of n, where n is the number of methylene groups in the side chain (Fig. 5a,b). The data shows that the $C_{p,m}$ values increase linearly with increasing n in the temperature range studied. The experimental and computational increments were compared in Fig. S37.

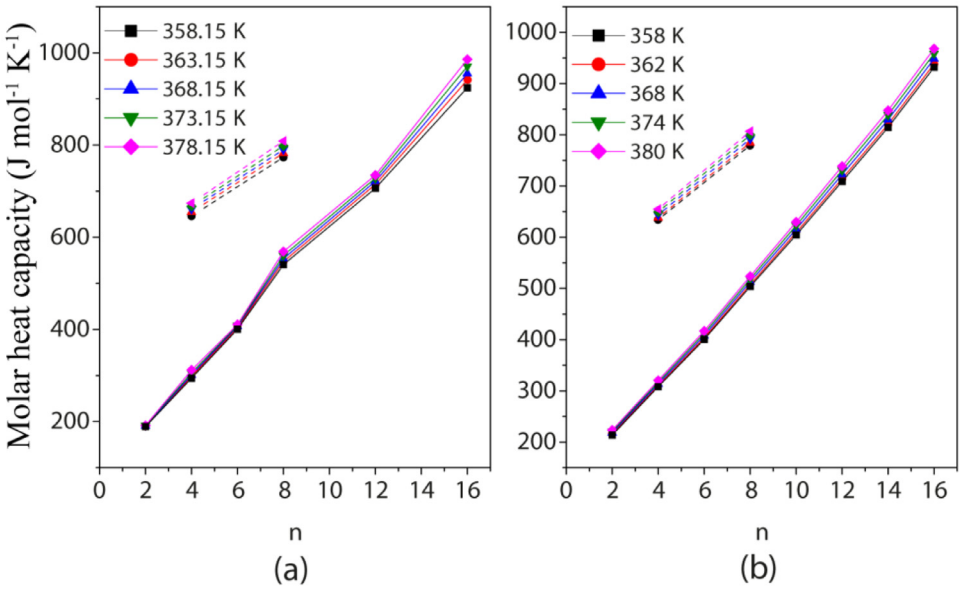

Fig. 5. **(a)** Experimental molar heat capacities (J mol^{-1} K^{-1}) as a function of the number of $–CH_2–$ groups (n) in the side chain for the studied ILs C_nMIMBr (solid lines) and Di-C_nMIMBr_2 (dotted lines). **(b)** Simulated molar heat capacities (J mol^{-1} K^{-1}) as a function of the number of $–CH_2–$ groups (n) in the side chain for the studied ILs C_nMIMBr (solid lines) and Di-C_nMIMBr_2 (dotted lines).

For each additional $–CH_2–$ group we found an increment of approximately 56 J mol^{-1} K^{-1} ± 2 J mol^{-1} K^{-1} over the temperature range from experiments and an increment of approximately 52 J mol^{-1} K^{-1} ± 2 J mol^{-1} K^{-1} from molecular modeling (Fig. 5). Similar analysis was performed by Gómez et al. (2013) for the IL $C_nMimNTf_2$ at 298.15 K and the increment *per* additional $–CH_2–$ group was 35 J mol^{-1} K^{-1}. The authors observed that this increment increases with temperature (Paulechka et al., 2007; Ge et al., 2008). Considering that the temperature range in this study is at least 1.5 times higher than in the work of Gómez et al. (2013), and the increment value per methylene group reported here was 1.6 greater, these $C_{p,m}$ values seem reasonable. The increment in $C_{p,m}$ was calculated at different temperatures and the values observed were approximately (54, 55, 56, 57, 59) J mol^{-1} K^{-1} at (358.15, 363.15, 368.15, 373.15, 378.15) K, respectively (from Fig. 5a). Similar to Gómez et al. (2013), the influence on the heat capacity by the additional methylene groups is higher at greater temperatures and follows a linear trend (r = 0.999). When considering the dicationic ILs (Di-C_nMIMBr_2) with $n = 4$ to $n = 8$, the increment observed in the experimental heat capacity from additional methylene groups in the spacer chain is approximately 33 J mol^{-1} K^{-1} ± 0.7 J mol^{-1} K^{-1} per $–CH_2–$ group and the increment observed in the molecular modeling heat capacity is 37 J mol^{-1} K^{-1} ± 0.9 J mol^{-1} K^{-1} per $–CH_2–$ group. This increment also increases with temperature, but with a smaller magnitude than for monocationic ILs - when considering the same temperatures, the increment to the dicationic ILs was approximately (32, 32, 32, 33, 34) J mol^{-1} K^{-1}, respectively (from Fig. 5). Since our scope of dicationic ILs was limited, it is hard to say that this is the general trend, but it can be said that the increment is apparently lower than for the monocationic ILs. The overall trend we observed is consistent with the literature showing that the longer the length of the alkyl chain or the higher the molecular mass, the higher the heat capacity. Also, the influence on the heat capacity of additional methylene groups is greater at higher temperatures for both mono- and dicationic ILs (Kim et al., 2004b; Cadena et al., 2006).

4. Conclusions

In this work, the molar heat capacities of a series of ionic liquids C_nMIMBr (n = 2, 4, 6, 8, 12, 16) and Di-C_nMIMBr_2 (n = 4, 8) was measured by Modulated Differential Scanning Calorimetry (MDSC) over the temperature range (358.15 to 378.15) K. The increase in heat capacity with temperature was linear for all ILs (r = 0.999). The increase in heat capacity with the number of methylene groups in the side chain of monocationic ILs was 56 J mol^{-1} K^{-1} ± 2 J mol^{-1} K^{-1}. For the dicationic ILs the increase was 33 J mol^{-1} K^{-1} ± 0.7 J mol^{-1} K^{-1} per $–CH_2–$ group. The experimental values were compared with those obtained from predictive models and molecular modeling analysis. Results from the predictive models were mixed, with reasonable agreement for monocationic ILs with alkyl side chain lengths from $n = 4$ to 12, showing the limitations of this heat capacity prediction approach. The dicationic ILs had values of $C_{p,m}$ in good accordance with the predictive models. The molecular modeling analysis of C_nMIMBr (n = 2, 4, 6, 8, 10, 12, 14, 16) and Di-C_nMIMBr_2 (n = 4, 8) showed good agreement with the experimental heat capacities, where the observed experimental trends of the increase in heat capacity with molecular mass and chain length were precisely captured by molecular modeling. This molecular modeling technique can be used to predict the heat capacity of other ILs such as ILs with the same anion with different C_nMIM^+ or Di-C_nMIM^{2+} type cations, or other IL systems that show a linear trend of increasing heat capacity with chain length or molecular weight. The samples used for the C_p measurements presented a water content greater than the values in the majority of published works, however, good agreements were found with literature and, when that was not the case, the water content did not seem to be the major factor influencing the differences. The results reported here may be useful for the development of new applications of long alkyl chain imidazolium-based ILs in processes operating at relatively high temperatures such as the temperatures used in this study and when completely drying the ILs is too laborious.

Declaration of Competing Interest

There is nothing to declare.

CRediT authorship contribution statement

Clarissa P. Frizzo: Conceptualization, Investigation, Resources, Writing – original draft, Supervision, Project administration, Funding acquisition. **Jean C.B. Vieira:** Methodology, Formal analysis, Validation, Investigation, Writing – original draft. **Dineli T.S. Ranathunga:** Methodology, Validation, Formal analysis, Writing – original draft. **Steven O. Nielsen:** Investigation, Resources, Writing – original draft. **Marcos A. Villetti:** Conceptualization, Investigation, Resources, Writing – original draft.

Data availability

Data will be made available on request.

Acknowledgments

The authors are thankful for the financial support from: the National Council of Scientific and Technological Development (Conselho Nacional de Desenvolvimento Científico e Tecnológico — CNPq) — proc. no. 403.134/2021-8); and the Rio Grande do Sul State Foundation for Research Support (Fundação de Amparo à Pesquisa do Estado do Rio Grande do Sul — FAPERGS) — grant no. 19/2551-0002273-5. The fellowships from CNPq (grant no. 311608/2021-3 for C.P.F.) and CAPES (for J.C.B.V.) are also acknowledged. This study was partly financed by the Coordination for the Improvement of Higher Education Personnel (Coordenação de Aperfeiçoamento de Pessoal de Nível Superior — CAPES) — Finance Code 001. S.O.N. and D.T.S.R. acknowledge the Texas Advanced Computing Center (TACC) at The University of Texas at Austin for providing HPC resources.

Supplementary materials

Supplementary material associated with this article can be found, in the online version, at doi:10.1016/j.jil.2022.100048.

References

Ahmadi, A., Haghbakhsh, R., Raeissi, S., Hemmati, V., 2015. A simple group contribution correlation for the prediction of ionic liquid heat capacities at different temperatures. Fluid Ph. Equilib. 403, 95–103. doi:10.1016/j.fluid.2015.06.009.

Anderson, J.L., Ding, R., Ellern, A., Armstrong, D.W., 2005. Structure and properties of high stability geminal dicationic ionic liquids. J. Am. Chem. Soc. 127, 593–604. doi:10.1021/ja046521u.

Aparicio, S., Atilhan, M., Karadas, F., 2010. Thermophysical properties of pure ionic liquids: review of present situation. Ind. Eng. Chem. Res. 49, 9580–9595. doi:10.1021/ie101441s.

Bedrov, D., Piquemal, J.P., Borodin, O., MacKerell, A.D., Roux, B., Schröder, C., 2019. Molecular dynamics simulations of ionic liquids and electrolytes using polarizable force fields. Chem. Rev. 119 (13), 7940–7995. doi:10.1021/acs.chemrev.8b00763.

Bender, C.R., 2014. Efeito dos Ânions de Líquidos iônicos Dicatiônicos na Formação de Agregados em Solução. Federal University of Santa Maria, Brazil.

Bender, C.R., Kuhn, B.L., Farias, C.A.A., Ziembowicz, F.I., Beck, T.S., Frizzo, C.P., 2019. Thermal stability and kinetic of decomposition of mono- And dicationic imidazolium-based ionic liquids. J. Braz. Chem. Soc. 30, 2199–2209. doi:10.21577/0103-5053.20190114.

Bendová, M., Wagner, Z., Bogdanov, M.G., Canji, M., Zdolsek, N., 2020. Heat capacity of 1-hexadecyl-3-methylimidazolium based ionic liquids in solid and liquid phase. J. Mol. Liq. 305, 112847. doi:10.1016/j.molliq.2020.112847.

Cadena, C., Zhao, Q., Snurr, R.Q., Maginn, E.J., 2006. Molecular modeling and experimental studies of the thermodynamic and transport properties of pyridinium-based ionic liquids. J. Phys. Chem. B 110, 821–832. doi:10.1021/jp056235k.

Calvar, N., Gómez, E., Macedo, E.A., Domínguez, Á., 2013. Thermal analysis and heat capacities of pyridinium and imidazolium ionic liquids. Thermochim. Acta 565, 178–182. doi:10.1016/j.tca.2013.05.007.

Červinka, C., Beran, G.J.O., 2017. Ab initio thermodynamic properties and their uncertainties for crystalline α-methanol. Phys. Chem. Chem. Phys. 19, 29940–29953. doi:10.1039/C7CP06605H.

Chaban, V.V., Voroshylova, I.V., Kalugin, O.N., 2011. A new force field model for the simulation of transport properties of imidazolium-based ionic liquids. Phys. Chem. Chem. Phys. 13, 7910. doi:10.1039/C0CP02778B.

Crosthwaite, J.M., Muldoon, M.J., Dixon, J.K., Anderson, J.L., Brennecke, J.F., 2005. Phase transition and decomposition temperatures, heat capacities and viscosities of pyridinium ionic liquids. J. Chem. Thermodyn. 37, 559–568. doi:10.1016/j.jct.2005.03.013.

Curtiss, L.A., Redfern, P.C., Raghavachari, K., Pople, J.A., 1998. Assessment of Gaussian-2 and density functional theories for the computation of ionization potentials and electron affinities. J. Chem. Phys. 109, 42–55. doi:10.1063/1.476538.

Diedrichs, A., Gmehling, J., 2006. Measurement of heat capacities of ionic liquids by differential scanning calorimetry. Fluid Phase Equilib. 244, 68–77. doi:10.1016/j.fluid.2006.03.015.

Doherty, B., Zhong, X., Gathiaka, S., Li, B., Acevedo, O., 2017. Revisiting OPLS force field parameters for ionic liquid simulations. J. Chem. Theory Comput. 13, 6131–6145. doi:10.1021/acs.jctc.7b00520.

Dommert, F., Wendler, K., Berger, R., Delle Site, L., Holm, C., 2012. Force fields for studying the structure and dynamics of ionic liquids: a critical review of recent developments. ChemPhysChem 13, 1625–1637. doi:10.1002/cphc.201100997.

Fakhraee, M., Zandkarimi, B., Salari, H., Gholami, M.R., 2014. Hydroxyl-functionalized 1-(2-Hydroxyethyl)-3-methyl Imidazolium ionic liquids: thermodynamic and structural properties using molecular dynamics simulations and *ab initio* calculations. J. Phys. Chem. B 118, 14410–14428. doi:10.1021/jp5083714.

Fakhraee, M., Gholami, M.R., 2015. Biodegradable ionic liquids: effects of temperature, alkyl side-chain length, and anion on the thermodynamic properties and interaction energies as determined by molecular dynamics simulations coupled with *ab initio* calculations. Ind. Eng. Chem. Res. 54, 11678–11700. doi:10.1021/acs.iecr.5b03199.

Farahani, N., Gharagheizi, F., Mirkhani, S.A., Tumba, K., 2013. A simple correlation for prediction of heat capacities of ionic liquids. Fluid Phase Equilib. 337, 73–82. doi:10.1016/j.fluid.2012.09.030.

Fredlake, C.P., Crosthwaite, J.M., Hert, D.G., Aki, S.N.V.K., Brennecke, J.F., 2004. Thermophysical properties of imidazolium-based ionic liquids. J. Chem. Eng. Data 49, 954–964. doi:10.1021/je034261a.

Frenkel, D., Smith, B., 1996. Understanding Molecular Simulation. From Algorithms to Applications. Academic Press, New York.

Frisch, MJ, Trucks, GW, Schlegel, HB, et al., 2016. Gaussian 16 Package. Gaussian, Inc, Wallingford, CT.

Frizzo, C.P., Bender, C.R., Gindri, I.M., Salbego, P.R.S., Villetti, M.A., Martins, M.A.P., 2015a. Anion effect on the aggregation behavior of the long-chain spacers dicationic imidazolium-based ionic liquids. Colloid. Polym. Sci. 293, 2901–2910. doi:10.1007/s00396-015-3680-y.

Frizzo, C.P., Bender, C.R., Tier, A.Z., Gindri, I.M., Salbego, P.R.S., Meyer, A.R., Martins, M.A.P., 2015b. Energetic and topological insights into the supramolecular structure of dicationic ionic liquids. CrystEngComm 17, 2996–3004. doi:10.1039/c5ce00073d.

Gardas, R.L., Coutinho, J.A.P., 2008. A group contribution method for heat capacity estimation of ionic liquids. Ind. Eng. Chem. Res. 47, 5751–5757. doi:10.1021/ie800330v.

Ge, R., Hardacre, C., Jacquemin, J., Nancarrow, P., Rooney, D.W., 2008. Heat capacities of ionic liquids as a function of temperature at 0.1 MPa. Measurement and prediction. J. Chem. Eng. Data 53, 2148–2153. doi:10.1021/je800335v.

Gindri, I.M., Frizzo, C.P., Bender, C.R., Tier, A.Z., Martins, M.A.P., Villetti, M.A., Machado, G., Rodriguez, L.C., Rodrigues, D.C., 2014. Preparation of TiO2 nanoparticles coated with ionic liquids: a supramolecular approach. ACS Appl. Mater. Interfaces 6, 11536–11543. doi:10.1021/am5022107.

Gómez, E., Calvar, N., Domínguez, Á., MacEdo, E.A., 2013. Thermal analysis and heat capacities of 1-alkyl-3-methylimidazolium ionic liquids with NTf2 -, TFO-, and DCA-anions. Ind. Eng. Chem. Res. 52, 2103–2110. doi:10.1021/ie3012193.

Gross, A.S., Bell, A.T., Chu, J., 2011. Thermodynamics of cellulose solvation in water and the ionic liquid 1-butyl-3-methylimidazolim chloride. J. Phys. Chem. B 115, 13433–13440. doi:10.1021/jp202415v.

Han, X., Armstrong, D.W., 2007. Ionic liquids in separations. Acc. Chem. Res. 40, 1079–1086. doi:10.1021/ar700044y.

Hapiot, P., Lagrost, C., 2008. Electrochemical reactivity in room-temperature ionic liquids. Chem. Rev. 108, 2238–2264. doi:10.1021/cr0680686.

Hennemann, B.L., Bender, C.R., Salbego, P.R.S., Meyer, A.R., Belladona, A.L., Zanatta, N., Bonacorso, H.G., Villetti, M.A., Martins, M.A.P., Frizzo, C.P., 2018. Models for understanding the structural effects on the cation-anion interaction strength of dicationic ionic liquids. J. Mol. Liq. 252, 184–193. doi:10.1016/j.molliq.2017.12.110.

Hernández-Ríos, S., Sánchez-Badillo, J., Gallo, M., López-Albarran, P., Gaspar-Armenta, J., González-García, R., 2017. Thermodynamic properties of the 1-butyl-3-methylimidazolium mesilate ionic liquid [C4mim][OMs] in condensed phase, using molecular simulations. J. Mol. Liq. 244, 422–432. doi:10.1016/j.molliq.2017.09.031.

Hu, H., Soriano, A.N., Leron, R.B., Li, M., 2011. Molar heat capacity of four aqueous ionic liquid mixtures. Thermochim. Acta 519, 44–49. doi:10.1016/j.tca.2011.02.027.

Humphrey, W., Dalke, A., Schulten, K., 1996. VMD: visual molecular dynamics. J. Mol. Graph 14, 33–38. Available from https://linkinghub.elsevier.com/retrieve/pii/0263785596000185.

Inoue, T., Dong, B., Zheng, L., 2007. Phase behavior of binary mixture of 1-dodecyl-3-methylimidazolium bromide and water revealed by differential scanning calorimetry and polarized optical microscopy. J. Colloid Interface Sci. 307, 578–581. doi:10.1016/j.jcis.2006.12.063.

Irikura, K.K., 2002. Thermo.pl. National Institute of Standards and Technology.

Ishii, Y., Matubayasi, N., 2020. Self-consistent scheme combining MD and order-N DFT methods: an improved set of nonpolarizable force fields for ionic liquids. J. Chem. Theory Comput. 16 (1), 651–665. doi:10.1021/acs.jctc.9b00793.

Ishii, Y., Matubayasi, N., Washizu, H., 2022. Nonpolarizable force fields through the self-consistent modeling scheme with MD and DFT methods: from ionic liquids to self-assembled ionic liquid crystals. J. Phys. Chem. B 126 (24), 4611–4622. doi:10.1021/acs.jpcb.2c02782.

Johnson III, R.D., 2020. Comparison of heat capacities at 298.15K for H_2O (Water). NIST Comput. Chem. Comp. Benchmark Database. Available from: https://cccbdb.nist.gov/introx.asp.

Kam, H.C., Ranathunga, D.T.S., Payne, E.R., Smaldone, R.A., Nielsen, S.O., Dodani, S.C., 2019. Spectroscopic characterization and in silico modelling of polyvinylpyrrolidone as an anion-responsive fluorescent polymer in aqueous media. Supramol. Chem. 31, 514–522. doi:10.1080/10610278.2019.1630740.

Kim, K., Shin, B., Lee, H., 2004a. Physical and electrochemical properties of 1-butyl-3-methylimidazolium bromide, 1-butyl-3-methylimidazolium iodide, and 1-butyl-3-methylimidazolium tetrafluoroborate. Korean J. Chem. Eng. 21, 1010–1014. doi:10.1007/BF02705586.

Kim, K., Shin, B., Lee, H., Ziegler, F., 2004b. Refractive index and heat capacity of 1-butyl-3-methylimidazolium bromide and 1-butyl-3-methylimidazolium tetrafluoroborate, and vapor pressure of binary systems for 1-butyl-3-methylimidazolium bromide + trifluoroethanol and 1-butyl-3-methylimidazolium tetrafluoroborate + trifluoroethanol. Fluid Phase Equilib. 218, 215–220. doi:10.1016/j.fluid.2004.01.002.

Kohagen, M., Brehm, M., Thar, J., Zhao, W., Müller-Plathe, F., Kirchner, B., 2011. Performance of quantum chemically derived charges and persistence of ion cages in ionic liquids. a molecular dynamics simulations study of 1- n -butyl-3-methylimidazolium bromide. J. Phys. Chem. B 115, 693–702. doi:10.1021/jp109612k.

Kuhn, B.L., Osmari, B.F., Heinen, T.M., Bonacorso, H.G., Zanatta, N., Nielsen, S.O., Ranathunga, D.T.S., Villetti, M.A., Frizzo, C.P., 2020. Dicationic imidazolium-based dicarboxylate ionic liquids: thermophysical properties and solubility. J. Mol. Liq. 308, 112983. doi:10.1016/j.molliq.2020.112983.

Liu, H., Maginn, E., Visser, A.E., Bridges, N.J., Fox, E.B., 2012. Thermal and transport properties of six ionic liquids: an experimental and molecular dynamics study. Ind. Eng. Chem. Res. 51, 7242–7254. doi:10.1021/ie300222a.

Lopes, J.N.C., Pádua, A.A.H., 2006. Molecular force field for ionic liquids III: Imidazolium, pyridinium, and phosphonium cations; chloride, bromide, and dicyanamide anions. J. Phys. Chem. B 110, 19586–19592. doi:10.1021/jp063901o.

MacFarlane, D.R., Forsyth, M., Howlett, P.C., Pringle, J.M., Sun, J., Annat, G., Neil, W., Izgorodina, E.I., 2007. Ionic liquids in electrochemical devices and processes: managing interfacial electrochemistry. Acc. Chem. Res. 40, 1165–1173. doi:10.1021/ar7000952.

Martins, M.A.P., Frizzo, C.P., Tier, A.Z., Moreira, D.N., Zanatta, N., Bonacorso, H.G., 2014. Update 1 of: ionic liquids in heterocyclic synthesis. Chem. Rev. 114, PR1–PR70. doi:10.1021/cr500106x.

Martínez, L., Andrade, R., Birgin, E.G., Martínez, J.M., 2009. PACKMOL: a package for building initial configurations for molecular dynamics simulations. J. Comput. Chem. 30, 2157–2164. doi:10.1002/jcc.21224.

McDaniel, J.G., Choi, E., Son, C.Y., Schmidt, J.R., Yethiraj, A., 2016. *Ab initio* force fields for imidazolium-based ionic liquids. J. Phys. Chem. B 120, 7024–7036. doi:10.1021/acs.jpcb.6b05328.

Mondal, A., Balasubramanian, S., 2014. A molecular dynamics study of collective transport properties of imidazolium-based room-temperature ionic liquids. J. Chem. Eng. Data 59, 3061–3068. doi:10.1021/je500132u.

Moosavi, M, Khashei, F., Sharifi, A., Mirzaei, M., 2017. The effects of temperature and alkyl chain length on the density and surface tension of the imidazolium-based geminal dicationic ionic liquids. J. Chem. Thermodyn. 107, 1–7. doi:10.1016/j.jct.2016.12.009.

Nasrabadi, A.T., Gelb, L.D., 2017. Structural and transport properties of tertiary ammonium triflate ionic liquids: a molecular dynamics study. J. Phys. Chem. B 121, 1908–1921. doi:10.1021/acs.jpcb.6b12418.

Neverov, V.S., Komolkin, A.V., 2010. A study of the structural and thermodynamic properties of water by the molecular dynamics method. Russ. J. Phys. Chem. B 4, 217–226. doi:10.1134/S1990793110020065.

Osborne, N.S., Stimson, H.F., Ginnings, D.C., 1934. Measurements of heat capacity and heat of vaporization of water in the range 0 degrees to 100 degrees C. J. Res. Natl. Bur. Stand 23, 197. Available from https://nvlpubs.nist.gov/nistpubs/jres/23/jresv23n2p197_A1b.pdf.

Paulechka, Y.U., Blokhin, A.V., Kabo, G.J., Strechan, A.A., 2007. Thermodynamic properties and polymorphism of 1-alkyl-3-methylimidazolium bis(triflamides). J. Chem. Thermodyn. 39, 866–877. doi:10.1016/j.jct.2006.11.006.

Paulechka, Y.U., Kabo, G.J., Blokhin, A.V., Shaplov, A.S., Lozinskaya, E.I., Vygodskii, Y.S., 2007. Thermodynamic properties of 1-alkyl-3-methylimidazolium bromide ionic liquids. J. Chem. Thermodyn. 39, 158–166. doi:10.1016/j.jct.2006.05.008.

Paulechka, Y.U., Kabo, G.J., Emel'yanenko, V.N., 2008. Structure, conformations, vibrations, and ideal-gas properties of 1-Alkyl-3-methylimidazolium bis(trifluoromethylsulfonyl)imide ionic pairs and constituent Ions. J. Phys. Chem. B 112, 15708–15717. doi:10.1021/jp804607n.

Paulechka, Y.U., 2010. Heat capacity of room-temperature ionic liquids: a critical review. J. Phys. Chem. Ref. Data 39, 033108. doi:10.1063/1.3463478.

Paulechka, Y.U., Kabo, A.G., Blokhin, A.V., Kabo, G.J., Shevelyova, M.P., 2010. Heat capacity of ionic liquids: Experimental determination and correlations with molar volume. J. Chem. Eng. Data 55, 2719–2724. doi:10.1021/je900974u.

Phillips, J.C., Braun, R., Wang, W., Gumbart, J, Tajkhorshid, E, Villa, E, et al., 2005. Scalable molecular dynamics with NAMD. J. Comput. Chem. [Internet] 26, 1781–1802. doi:10.1002/jcc.20289.

Ren, P., Ponder, J.W., 2004. Temperature and pressure dependence of the AMOEBA water model. J. Phys. Chem. B 108 (35), 13427–13437. doi:10.1021/jp0484332.

Rostami, A., Hemmati-Sarapardeh, A., Karkevandi-Talkhooncheh, A., Husein, M.M., Shamshirband, S., Rabczuk, T., 2019. Modeling heat capacity of ionic liquids using group method of data handling: A hybrid and structure-based approach. Int. J. Heat Mass Transf. 129, 7–17. doi:10.1016/j.ijheatmasstransfer.2018.09.057.

Roy, T.K., Gerber, R.B., 2013. Vibrational self-consistent field calculations for spectroscopy of biological molecules: new algorithmic developments and applications. Phys. Chem. Chem. Phys. 1, 9468. doi:10.1039/C3CP50739D.

Scott, A.P., Radom, L., 1996. Harmonic vibrational frequencies: an evaluation of Hartree−Fock, Møller−Plesset, quadratic configuration interaction, density functional theory, and semiempirical scale factors. J. Phys. Chem. 100, 16502–16513. doi:10.1021/jp960976r.

Shirota, H., Mandai, T., Fukazawa, H., Kato, T., 2011. Comparison between dicationic and monocationic ionic liquids: liquid density, thermal properties, surface tension, and shear viscosity. J. Chem. Eng. Data 56, 2453–2459. doi:10.1021/je2000183.

Sinha, P., Boesch, S.E., Gu, C., Wheeler, R.A., Wilson, A.K., 2004. Harmonic vibrational frequencies: scaling factors for HF, B3LYP, and MP2 methods in combination with correlation consistent basis sets. J. Phys. Chem. A 108, 9213–9217. doi:10.1021/jp048233q.

Sprenger, K.G., Jaeger, V.W., Pfaendtner, J., 2015. The General AMBER Force Field (GAFF) can accurately predict thermodynamic and transport properties of many ionic liquids. J. Phys. Chem. B 119, 5882–5895. doi:10.1021/acs.jpcb.5b00689.

Steudte, S., Bemowsky, S., Mahrova, M., Bottin-Weber, U., Tojo-Suarez, E., Stepnowski, P., Stolte, S., 2014. Toxicity and biodegradability of dicationic ionic liquids. RSC Adv. 4, 5198–5205. doi:10.1039/C3RA45675G.

Tan, X., Zhang, J., Luo, T., Sang, X., Liu, C., Zhang, B., Peng, L., Li, W., Han, B., 2016. Micellization of long-chain ionic liquids in deep eutectic solvents. Soft Matter 12, 5297–5303. doi:10.1039/C6SM00924G.

Tenney, C.M., Massel, M., Mayes, J.M., Sen, M., Brennecke, J.F., Maginn, E.J., 2014. A computational and experimental study of the heat transfer properties of nine different ionic liquids. J. Chem. Eng. Data 59, 391–399. doi:10.1021/je400858t.

Theodorakis, P.E., Hsu, H., Paul, W., Binder, K., 2011. Computer simulation of bottle-brush polymers with flexible backbone: Good solvent versus theta solvent conditions. J. Chem. Phys. 135, 164903. doi:10.1063/1.3656072.

Turner, E.A., Pye, C.C., Singer, R.D., 2003. Use of *ab initio* calculations toward the rational design of room temperature ionic liquids. J. Phys. Chem. A 107, 2277–2288. doi:10.1021/jp021694w.

Vega, C., Abascal, J.L.F., 2011. Simulating water with rigid non-polarizable models: a general perspective. Phys. Chem. Chem. Phys. 13, 19663. doi:10.1039/C1CP22168J.

Vieira, J.C.B., Paz, A.V., Hennemann, B.L., Kuhn, B.L., Bender, C.R., Meyer, A.R., Pagliari, A.B., Villetti, M.A., Frizzo, C.P., 2020. Effect of large anions in thermal properties and cation-anion interaction strength of dicationic ionic liquids. J. Mol. Liq. 298, 112077. doi:10.1016/j.molliq.2019.112077.

Wasserscheid, P., Welton, T., 2002. Ionic Liquids in Synthesis. Wiley-VCH Verlag, Stuttgart, Germany.

Welton, T., 1999. Room-temperature ionic liquids. solvents for synthesis and catalysis thomas. Chem. Rev. 99, 2071–2084. doi:10.1021/cr980032t.

Yan, T., Burnham, C.J., Del Pópolo, M.G., Voth, G.A., 2004. Molecular dynamics simulation of ionic liquids: the effect of electronic polarizability. J. Phys. Chem. B 108, 11877–11881. doi:10.1021/jp047619y.

Youngs, T.G.A., Hardacre, C., 2008. Application of static charge transfer within an ionic-liquid force field and its effect on structure and dynamics. ChemPhysChem 9, 1548–1558. doi:10.1002/cphc.200800200.

Yu, Y.H., Soriano, A.N., Li, M.H., 2009. Heat capacities and electrical conductivities of 1-n-butyl-3-methylimidazolium-based ionic liquids. Thermochim. Acta 482, 42–48. doi:10.1016/j.tca.2008.10.015.

Zeng, S., Zhang, X., Bai, L., Zhang, X., Wang, H., Wang, J., Bao, D., Li, M., Liu, X., Zhang, S., 2017. Ionic-liquid-based CO_2 capture systems: structure, interaction and process. Chem. Rev. 117, 9625–9673. doi:10.1021/acs.chemrev.7b00072.

Zhang, H., Li, M., Yang, B., 2018. Design, synthesis, and analysis of thermophysical properties for imidazolium-based geminal dicationic ionic liquids. J. Phys. Chem. C 122, 2467–2474. doi:10.1021/acs.jpcc.7b09315.

Zhang, H., Liu, J., Li, M., Yang, B., 2018. Functional groups in geminal imidazolium ionic compounds and their influence on thermo-physical properties. J. Mol. Liq. 269, 738–745. doi:10.1016/j.molliq.2018.08.037.

Zhang, H., Xu, W., Liu, J., Li, M., Yang, B., 2019. Thermophysical properties of dicationic imidazolium-based ionic compounds for thermal storage. J. Mol. Liq. 282, 474–483. doi:10.1016/j.molliq.2019.03.012.

Zhong, X., Liu, Z., Cao, D., 2011. Improved classical united-atom force field for imidazolium-based ionic liquids: tetrafluoroborate, hexafluorophosphate, methylsulfate, trifluoromethylsulfonate, acetate, trifluoroacetate, and bis(trifluoromethylsulfonyl)amide. J. Phys. Chem. B 115, 10027–10040. doi:10.1021/jp204148q.

Zhou, Y., Antonietti, M., 2003. Preparation of highly ordered monolithic supermicroporous lamellar silica with a room-temperature ionic liquid as template via the nanocasting technique. Adv. Mater. 15, 1452–1455. doi:10.1002/adma.200305265.

Zhu, J., Bai, L., Chen, B., Fei, W., 2009. Thermodynamical properties of phase change materials based on ionic liquids. Chem. Eng. J. 147, 58–62. doi:10.1016/j.cej.2008.11.016.